

Interpreting the *Spitzer*/IRAC Colours of $7 \leq z \leq 9$ Galaxies: Distinguishing Between Line Emission and Starlight Using ALMA

G. W. Roberts-Borsani^{1,2*}, R. S. Ellis² and N. Laporte^{3,4,2}

¹*Department of Physics and Astronomy, University of California, Los Angeles, 430 Portola Plaza, Los Angeles, CA 90095, USA*

²*Department of Physics and Astronomy, University College London, Gower Street, London WC1E 6BT, UK*

³*Kavli Institute for Cosmology, University of Cambridge, Madingley Road, Cambridge CB3 0HA, UK*

⁴*Cavendish Laboratory, University of Cambridge, 19 JJ Thomson Avenue, Cambridge CB3 0HE, UK*

Accepted XXX. Received YYY; in original form ZZZ

ABSTRACT

Prior to the launch of JWST, *Spitzer*/IRAC photometry offers the only means of studying the rest-frame optical properties of $z > 7$ galaxies. Many such high redshift galaxies display a red [3.6] - [4.5] micron colour, often referred to as the “IRAC excess”, which has conventionally been interpreted as arising from intense [O III]+H β emission within the [4.5] micron bandpass. An appealing aspect of this interpretation is similarly intense line emission seen in star-forming galaxies at lower redshift as well as the redshift-dependent behaviour of the IRAC colours beyond $z \sim 7$ modelled as the various nebular lines move through the two bandpasses. In this paper we demonstrate that, given the photometric uncertainties, established stellar populations with Balmer (4000 Å rest-frame) breaks, such as those inferred at $z > 9$ where line emission does not contaminate the IRAC bands, can equally well explain the redshift-dependent behaviour of the IRAC colours in $7 \lesssim z \lesssim 9$ galaxies. We discuss possible ways of distinguishing between the two hypotheses using ALMA measures of [O III] 88 micron and dust continuum fluxes. Prior to further studies with JWST, we show that the distinction is important in determining the assembly history of galaxies in the first 500 Myr.

Key words: galaxies: evolution – galaxies: high-redshift – cosmology: reionization – cosmology: early Universe

1 INTRODUCTION

The last few years has seen impressive progress in studies of galaxies in the so-called “reionisation era” corresponding to the redshift interval $7 < z < 10$. However, the number of spectroscopically-confirmed examples remains limited and much has been deduced from spectral energy distributions (SEDs) of photometric samples. In addition to demographic studies based on star formation rate densities (Oesch et al. 2014; McLeod et al. 2016) and luminosity functions (Atek et al. 2015; Bouwens et al. 2015), a key area of interest is studies of the gaseous and stellar properties of early systems. The latter topic is central to understand both the ionising capability of early galaxies as well as the age of their stellar populations (for a recent review see Stark 2016).

Although much of the progress has been made using photometric samples based on Hubble imaging, both in deep fields (Grogin et al. 2011; Koekemoer et al. 2011; Ellis et al. 2013) and through lensing clusters (Bradley et al. 2014; Lotz et al. 2017; Salmon et al. 2018; Coe et al. 2019), the *Spitzer Space Telescope* has made a key contribution since, at $z \gtrsim 5$, the two bandpasses at 3.6 and 4.5 μm sample the rest-frame optical. At redshifts of

$z \gtrsim 6.6$, it is claimed that the redshift-dependent trend of the IRAC colours is consistent with intense nebular emission lines shifting through the bandpasses (Labbé et al. 2013; Smit et al. 2015; Roberts-Borsani et al. 2016), although the precision of this exercise is dependent mostly on samples with only photometric redshifts. With this in mind, the surprising spectroscopic confirmation with Lyman- α (Oesch et al. 2015; Zitrin et al. 2015; Stark et al. 2017) of the 4 brightest $z > 7$ galaxies in the CANDELS survey selected to display red *Spitzer*/IRAC 3.6 μm -4.5 μm colours (and hence an “IRAC excess”) of > 0.5 mag (Roberts-Borsani et al. 2016), reinforced the hypothesis that the IRAC excess arises from intense [O III] 5007 Å plus H β emission within the 4.5 μm band. To explain the IRAC colours, the rest-frame equivalent widths (EWs) of [O III] must be of order 500 Å.

Although it will not be possible to confirm this suggestion with direct spectroscopy until the launch of JWST, the so-called “[O III] hypothesis” has been widely accepted for several reasons. Firstly, at lower redshift $z \sim 6.6$ where [O III] passes through the 3.6 μm bandpass, the required blue 3.6 μm -4.5 μm colour is seen for a sample of galaxies, several of which are now spectroscopically-confirmed with ALMA (Smit et al. 2018; see also Sobral et al. 2015, Pentericci et al. 2016, Matthee et al. 2017). Finally, as a proof of concept, galaxies whose rest-frame [O III] emission exceed

* E-mail: guidorb@astro.ucla.edu

$EW \approx 1000 \text{ \AA}$, while difficult to reproduce via modelling except in very young star-forming systems, have been studied at $z \approx 2$ (Maseda et al. 2014).

A more recent development has been the location of IRAC-excess galaxies whose photometric redshifts lie at $z > 9$; at these redshifts [O III] is shifted beyond both IRAC filters. Thus far only one system, MACS1149-JD1, hereafter JD1, has been spectroscopically-confirmed at $z=9.11$ (Hashimoto et al. 2018). Analysis of its SED attributes the IRAC excess to the Balmer break at 4000 \AA consistent with a mature $\sim 200\text{-}300$ Myr old stellar population providing a first tantalising glimpse of “cosmic dawn” at $z \approx 15 \pm 3$. This discovery raises the question of the extent to which the IRAC excess seen in galaxies at $7 < z < 9$ might also, in part, be due to a similar Balmer break. The distinction is important since it would imply many luminous $z \approx 7\text{-}9$ galaxies may have older stellar populations and larger stellar masses than previously thought, with interesting consequences for the presence of earlier star formation. An additional issue is whether JD1 is representative of the galaxy population at $z \approx 7 - 9$ (see Katz et al. 2019).

The goal of the present paper is to explore the extent to which an IRAC excess and its redshift-dependent trend might be due, in part, to starlight rather than solely intense [O III] line emission. A plan of the paper follows. In §2 we examine predicted IRAC colours in the context of both hypotheses, using carefully-chosen template galaxies as well as contemporary stellar population models that incorporate nebular line emission. In §3, we turn to what data might be needed to distinguish between the two hypotheses. Prior to spectroscopy with JWST, we consider the flux of [O III] $88 \mu\text{m}$ which is accessible with ALMA and examine the IRAC colour for those spectroscopically-confirmed galaxies for which [O III] $88 \mu\text{m}$ fluxes are available. In §4 we discuss our results and the implications on the early assembly of galaxies. Throughout this paper we refer to the *HST* F160W and *Spitzer*/IRAC 3.6 and 4.5 micron bands as H_{160} , [3.6] and [4.5], respectively, for simplicity. We also assume $H_0 = 70 \text{ km/s/Mpc}$, $\Omega_m = 0.3$, and $\Omega_\Lambda = 0.7$. All magnitudes are in the AB system (Oke & Gunn 1983).

2 MODELLING THE IRAC COLOURS OF $7 < Z < 9$ GALAXIES

In exploring the redshift-dependent behaviour of the IRAC 3.6 and $4.5 \mu\text{m}$ colours, under the hypotheses of contributions from [O III] line emission or a Balmer break due to a more mature stellar population, we begin by selecting two template SEDs fitted to actual data for spectroscopically-confirmed $z > 7$ galaxies. For the case of intense [O III] emission, we use a spectroscopic template fitted to the ground-based and *HST/Spitzer* photometry of EGSY8p7 at $z=8.68$ (Zitrin et al. 2015), one of the four IRAC-excess bright sources first identified in the CANDELS survey (Roberts-Borsani et al. 2016). The template and *HST/Spitzer* photometry used here are taken directly from the latter study and we refer the reader to that paper for details on the construction of the templates and derivation of the photometric data points.

Similarly, for the case of a mature stellar population with a prominent Balmer break, we select the SED fit to MACS1149-JD1 at $z=9.11$ from Hashimoto et al. (2018). This fit represents a composite of a mature $\sim 200\text{-}300$ Myrs population augmented with a younger component invoked to match the intensity of [O III] emission at $88 \mu\text{m}$ discovered with ALMA; full details can be found in Hashimoto et al. (2018). Since this spectral fit includes nebular line emission which, while not contributing significantly to the IRAC

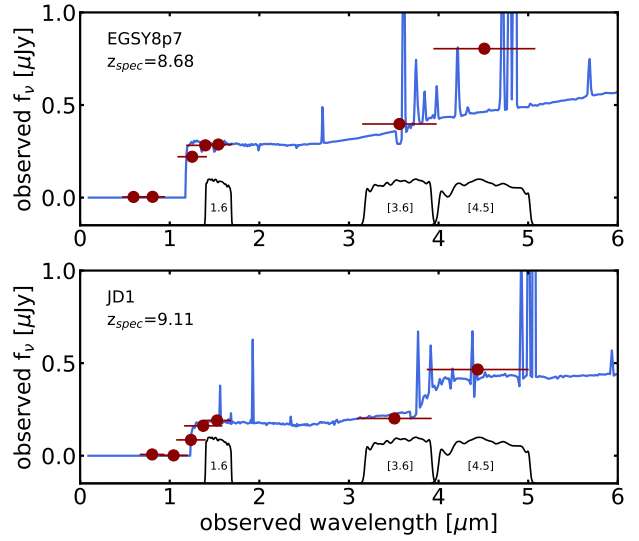


Figure 1. The two synthetic spectra (blue lines) and associated photometry (dark red points with error bars; Roberts-Borsani et al. 2016; Zheng et al. 2017) used in this study to demonstrate the similarity of the redshift-dependent *Spitzer*/IRAC [3.6]-[4.5] evolution. The spectra are of EGSY8p7 (Roberts-Borsani et al. 2016; Zitrin et al. 2015), a supposed extreme [O III]+H β line emitter at $z = 8.68$ (top), and JD1 (Hashimoto et al. 2018), a Balmer break galaxy at $z = 9.11$ (bottom). The JD1 spectrum shown here is uncorrected for magnification. Shown at the bottom of each panel are the *HST*/ H_{160} and *Spitzer*/IRAC 3.6 μm and 4.5 μm response filters, for reference.

bands at $z > 9$ will do so at lower redshift, we also explore the effect of suppressing all optical emission lines from the fitted spectrum of JD1. The observed EWs of the combined [O III] and H β lines are $EW([O III]+H\beta) \approx 6690 \text{ \AA}$ and $EW([O III]+H\beta) \approx 3408 \text{ \AA}$ for EGSY8p7 and JD1, respectively.

The adopted spectral templates and associated photometry are shown in Figure 1, and for all subsequent analysis, we normalise both spectra by their flux at $0.325 \mu\text{m}$ (rest-frame), where the spectra are free from emission or absorption features, in order to ensure their 3.6 μm and 4.5 μm photometry can be directly compared.

We are now in a position to explore how these template spectra affect the IRAC colours over the redshift range $7 < z < 9$. In Figure 2 we present the redshift evolution of the [3.6]-[4.5] and H_{160} -[3.6] colours in steps of $\Delta z = 0.05$ for each of our fiducial spectra, following a similar approach by Labbé et al. (2013). At each redshift interval, the colours are measured directly from the redshifted spectrum using the relevant filter response curves. The simulation shows that the Balmer break in JD1 can mimic the effect of intense line emission to within ± 0.1 mag in the [3.6]-[4.5] colour, particularly at redshifts $z \gtrsim 7.5$, and even produce redder colours at $z \gtrsim 8.5$. Since the JD1 template includes a contribution from nebular emission lines (e.g., [O II], H β and [O III]), including some from H β and [O III] 44959 \AA at $z=9.11$ in the $4.5 \mu\text{m}$ band, we explored suppressing all optical line emission in this template but find consistently red IRAC colours with virtually identical colour-colour evolution (particularly at $z \gtrsim 8$) and little difference in normalisation (the masked spectrum consistently produces red IRAC [3.6]-[4.5] colours $\lesssim 0.2$ mag lower than its unmasked counterpart) on the simulated colours (see discussion below and Figure 2).

The similarity between the redshift-dependent trends of a

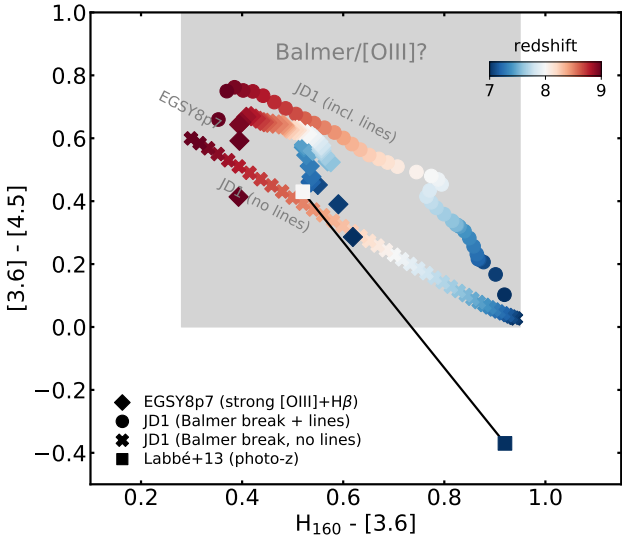


Figure 2. The $[3.6] - [4.5]$ vs $H_{160} - [3.6]$ colours as a function of redshift from $7 \leq z \leq 9$ for the spectral templates of spectroscopically-confirmed galaxies EGSY8p7 (diamonds; assumed to be an extreme $[O\text{III}]+H\beta$ emitter) and JD1 (circles; a Balmer break galaxy). Since the template of JD1 includes some optical nebular emission, we also show the results for JD1 with masked emission lines (crosses) to highlight the contribution from the stellar continuum only. The gray shaded region indicates the colour space over which the different spectra produce similar colours for the selected redshift interval. Overplotted are the $z \sim 8$ and $z \sim 7$ results from stacked photometrically-selected galaxies from the study of Labbé et al. (2013), and the connecting vector (black line) between the two. A clear difference exists between spectroscopic and photometric results, for which blue *Spitzer/IRAC* colours at $z \sim 7$ may reflect contamination of the stack by strong nebular line emitters at $z \sim 6.6$.

Balmer break and intense line emission over the chosen redshift interval $7 < z < 9$ may seem surprising given earlier conclusions of a similar exercise undertaken by Labbé et al. (2013). Those authors explored the effect by analysing average SEDs (containing nebular emission lines) of photometrically-selected $z_{\text{phot}} \approx 7$ and $z_{\text{phot}} \approx 8$ galaxies. They were able to reproduce the $[3.6] - [4.5]$ and $H_{160} - [3.6]$ colours only with the presence of strong ($\text{EW}([O\text{III}]+H\beta) \sim 560\text{-}670 \text{ \AA}$) nebular emission lines, rejecting an increased dust content or stellar age. Their average $z \sim 7$ and $z \sim 8$ colours, as well as the connecting vector, are shown in Figure 2 together with our results. However, as can be seen using our templates based on *spectroscopically-confirmed* galaxies, the same overall trend and $[3.6] - [4.5]$ colours can also be reproduced by the JD1 Balmer break template. Throughout the redshift interval $7 < z < 9$, at no point does the $[3.6] - [4.5]$ colour drop below zero, in contrast to what Labbé et al. (2013) found at $z \sim 7$. Conceivably their average SED at $z=7$ was contaminated by a few $z \sim 6.6$ extreme line emitters now known to have extremely blue colours (Smit et al. 2015) due to contamination of the $3.6 \mu\text{m}$ band by $[O\text{III}]+H\beta$.

At this point we caution the reader that this exercise is not motivated to claim that the IRAC excess seen in many sources at $7 < z < 9$ cannot be due to intense $[O\text{III}]+H\beta$ emission. Rather, we wish to point out that the existence of a Balmer break for JD1 at $z > 9$ may imply *some contribution of starlight to the IRAC excess* seen in sources at $7 < z < 9$ and to explore whether such starlight is prominent in existing spectroscopically-confirmed galaxies at $7 < z < 9$. Of course, these results will depend on the

choice of spectral template. In the case of JD1 we selected the only case known to date of a galaxy with an IRAC excess which cannot be explained solely via intense line emission (Hashimoto et al. 2018). For the line emitter template, the results will differ slightly depending on which object is chosen from the samples available in the literature. Given this uncertainty plus recent discussions on the possible exceptional case of JD1 (Bingelli et al. 2019), it is helpful to examine the redshift-dependent trends produced by stellar population synthesis models as well as to expand the discussion to compare all these predictions with actual $z > 7$ data in the literature.

For the population synthesis models we use the Pégase3 suite (Fioc & Rocca-Volmerange 2019) which includes self-consistent modelling of nebular line emission and dust evolution. Clearly such models have an abundance of free parameters but, for the present exercise, our main goal is to demonstrate that *relative contributions* of synthetic galaxy spectra selected at various ages from a simple star formation history can also reproduce the trends we see using our observed spectral templates. For the current experiment, our simulated galaxy adopts a Chabrier (2003) IMF with a constant star formation history beginning at $z = 15$ and ending at $z = 2$. We select simulated spectra at various time intervals corresponding to galaxy ages from 1 Myr ($z \sim 15$) to 600 Myr ($z \sim 6$). Nebular emission and dust evolution are included in the modelling. As with the EGSY8p7 and JD1 spectra, the Pégase3 spectra are normalised to their flux at $0.325 \mu\text{m}$ (rest-frame) prior to analysis.

Figure 3 shows the IRAC $[3.6] - [4.5]$ colour versus redshift trend for our fiducial galaxy templates as well as the Pégase3 models. For each of our SEDs (i.e., EGSY8p7, JD1 and each of the Pégase spectra corresponding to various time intervals of the simulated galaxy's evolution), the spectrum is redshifted across our range of interest and the colour measured through the relevant response filters, in order to assess the *relative* colour contributions from each spectrum's features. The figure also shows the JD1 template adjusted to exclude the contribution from optical nebular lines. In order to compare with actual data, Table 1 represents a compilation of 12 $z > 7$ spectroscopically-confirmed galaxies drawn from the literature, each with available *HST* and *Spitzer/IRAC* photometry, and we plot their photometric data alongside the spectroscopic results in Figure 3. For completeness we also add four spectroscopically-confirmed $z \approx 6.8$ sources from the studies of Smit et al. (2018) and Laporte et al. (2017b) which demonstrate the influence of $[O\text{III}]+H\beta$ emission in the $3.6 \mu\text{m}$ band at lower redshift.

Focusing initially on the comparison between Pégase3 and our chosen galaxy templates, we can see very similar trends, albeit with some difference in normalisation. Within the $7 < z < 9$ redshift range, Pégase models corresponding to younger ages closely track the evolution of the EGSY8p7 template, whose red colours are dominated by strong nebular emission lines, whilst evolved stellar ages are required to explain the evolution of the JD1 templates (both with and without emission lines), where the red colour is primarily due to a Balmer break.

Considering next how the templates and synthesis models match the IRAC colours of 12 spectroscopically-confirmed $z > 7$ galaxies, we can see that line emission in both Pégase3 and the EGSY8p7 (line emitting) template are required to explain the strong dip in $[3.6] - [4.5]$ colour at $z \approx 6.6$ as indicated by Smit et al. (2018); as expected the JD1 template with masked emission lines has no dip. However, at higher redshift, where the $[O\text{III}]+H\beta$ lines enter the $4.5 \mu\text{m}$ band, the red colour is initially more easily reproduced by cases with strong line emission. For SEDs with a

flat continuum, as assumed by [Roberts-Borsani et al. \(2016\)](#), such a colour remains relatively constant until the lines leave the band at $z = 9$. However, in the case of a moderate to strong Balmer break and reduced (but not absent) line emission, the IRAC excess *increases* from $z \gtrsim 7.5$ onwards as the Balmer break moves redward, thereby removing flux from the $3.6\mu\text{m}$ band whilst simultaneously providing a relatively constant amount of flux in the $4.5\mu\text{m}$ band. In the case where the rest-frame optical continuum is not flat, this impacts the *slope* of the [3.6] - [4.5] colour evolution. The impact of the Balmer break is particularly evident when comparing the evolution of the masked JD1 spectrum to the older-aged Pégase3 synthesis models which, despite including (normal) emission lines display virtually identical [3.6] - [4.5] evolution.

Examining the actual data, one can reasonably securely conclude that the large IRAC excesses at $7 \lesssim z \lesssim 7.5$ (e.g. [Finkelstein et al. 2013](#); [Hashimoto et al. 2019](#)) are difficult to reproduce without an extreme [O III]+H β contribution, as is clearly the case for IRAC colours for the sources at $z \approx 6.8$ studied by [Smit et al. \(2018\)](#) and [Laporte et al. \(2017b\)](#). However, for the sources at $7.5 \lesssim z \lesssim 9$ (e.g., [Watson et al. 2015](#); [Tamura et al. 2019](#); [Laporte et al. 2017a](#) plus GN-z10-3 and EGSY8p7), the paucity of spectroscopic data makes it premature to conclude that the IRAC excess in galaxies beyond $z \approx 7$ arises entirely from line emission.

3 DISTINGUISHING BETWEEN A BALMER BREAK AND INTENSE LINE EMISSION WITH ALMA

In Section 2 we have shown that red *Spitzer*/IRAC [3.6]-[4.5] colours for galaxies lying between $7 < z < 9$ could arise from contributions of both intense nebular line emission and starlight. We now consider whether it is possible to break this degeneracy prior to the use of spectroscopy with JWST. ALMA observations with Band 7 targeting the [O III] $88\mu\text{m}$ line and dust continuum may provide a potential way forward. Using detailed SED modelling with synthetic spectra from Pégase3 we now investigate whether ALMA observations can place constraints on the contribution from young stars via [O III] $88\mu\text{m}$ emission and mature stellar populations from the presence of a dust continuum.

Currently, four of the 12 $z > 7$ spectroscopically-confirmed galaxies with *Spitzer*/IRAC excesses listed in Table 1 have the appropriate ALMA data: JD1, A2744_YD4, MACS0416_Y1 and B14-65666 (henceforth YD4, Y1 and B14 for convenience), see Table 2. To determine accurate SEDs, for each of the aforementioned galaxies we use the relevant references in Table 1 (and references therein) to compile *HST* ACS+WFC3/IR, (B_{435} , V_{606} , I_{814} , Y_{105} , J_{125} , JH_{140} and H_{160} bands), VLT/HAWK-I K_s , as well as *Spitzer*/IRAC [3.6] and [4.5] photometry. For B14 we use near-infrared z , Y , J , and H photometry from VISTA, in addition to data in the VLT/HAWK-I K_s and *Spitzer*/IRAC [3.6] and [4.5] bands. All *HST* upper limits and error bars represent 1σ uncertainties, whilst those redward of these are 2σ .

To evaluate the relative contributions of nebular emission lines and starlight we create a repertoire of Pégase3 spectra with which to fit the above data for the four spectroscopically-confirmed $z > 7$ galaxies. We generate mass-normalised galaxy spectra for a young component dominated by a recent burst of constant star formation with duration $\tau_{\text{young}}=10$ Myrs, and for a component with a less recent phase of constant star formation for a range of durations $\tau_{\text{old}}=[10, 50, 100, 200, 300, 400, 500]$ Myrs, where a Balmer break is allowed to form. We then extract spectra at 1 Myr intervals for the young component, and 20 Myr intervals from ages of 1 Myr to

the age of the Universe at the redshift of each galaxy for the older component. For simplicity, we assume emission lines arise from the young component only, since these come from star-forming regions and are not seen in mature stellar populations. These models are used, sometimes in combination (i.e. recent burst + earlier star formation), with a custom SED-fitting code in a Bayesian framework, to maximise the log-likelihood of the model given the data, including an analytical treatment of upper limits ([Sawicki 2012](#)). The free parameters of the code are the mass of the galaxy system, M_{sys} ¹ (one for each stellar component) and a multiplicative factor, L_{neb} , to scale the luminosity of the nebular emission lines, whose FWHM are fixed to that of the [O III] $88\mu\text{m}$ line presented in Table 2. The adopted priors are $\log M_{\text{sys}}=[5,15] M_{\odot}$ and $L_{\text{neb}}=[0,50]$, allowing for both normal and extreme nebular emission contributions.

To illustrate how the ALMA observations may differentiate between intense nebular emission and starlight in explaining the IRAC colours, we consider the case of YD4 since, for this source, all photometric points redward of the Lyman break and the ALMA spectroscopic constraints are robustly measured. First we fit the data with a single-component young model (permitting a dust contribution), once with *HST*+VLT/HAWK-I+*Spitzer*/IRAC data only and then again incorporating the ALMA Band 7 constraints. The best-fit SEDs are shown in Figure 4. The continuum fits to the *HST* and HAWK-I photometry are satisfactory and comparable in each case. However, there is a major difference in the predicted *Spitzer*/IRAC photometry. Ignoring the ALMA constraints, the IRAC excess demands the presence of strong nebular emission lines in which case the [O III] $88\mu\text{m}$ line is considerably overpredicted (by a factor ≈ 10 , not shown) and the continuum dust emission is similarly poorly matched. Additionally, the presence of nebular emission lines - namely the [O II] doublet at a rest-frame of $\sim 3730\text{\AA}$ - adds non-negligible boosting to the [3.6] band. Including the ALMA constraints, the nebular emission in the IRAC bands is modest, indicating the need for an additional component to fit these data, for example a Balmer break originating from star formation at earlier times.

We thus now proceed to fit all of the available data for each of the four galaxies with a two-component model comprising a contribution from young stars with intense nebular emission and an older stellar component. The two-component models are derived from all unique combinations of young and older spectra requiring only that $\text{age}_{\text{young}} < \text{age}_{\text{galaxy}} - \tau_{\text{old}}$ so that the recent burst of star formation from the young component occurs only when star formation in the older component has completed. In these two-component models, for simplicity, we assume the dust contributions arise only from the older component and specifically only if there is a Band 7 continuum detection. By comparing these two-component fits to those for a single-component (with dust included following the guidelines indicated above), we can determine, as suggested in the case of YD4, (i) whether the two-component fits are significantly better than the single young component ones and (ii) whether the first indicate the presence of an older, more mature stellar population.

The results of our best fit two-component models are presented in Figure 5, where we find generally good agreement with the observed photometric data sets and ALMA constraints. For two of the four galaxies (JD1 and YD4), the best-fit model correctly predicts the presence or upper limit of dust mass based on the ALMA

¹ For a proper definition of how this translates in the Pégase3 formalism to stellar mass, see [Fioc & Rocca-Volmerange 2019](#).

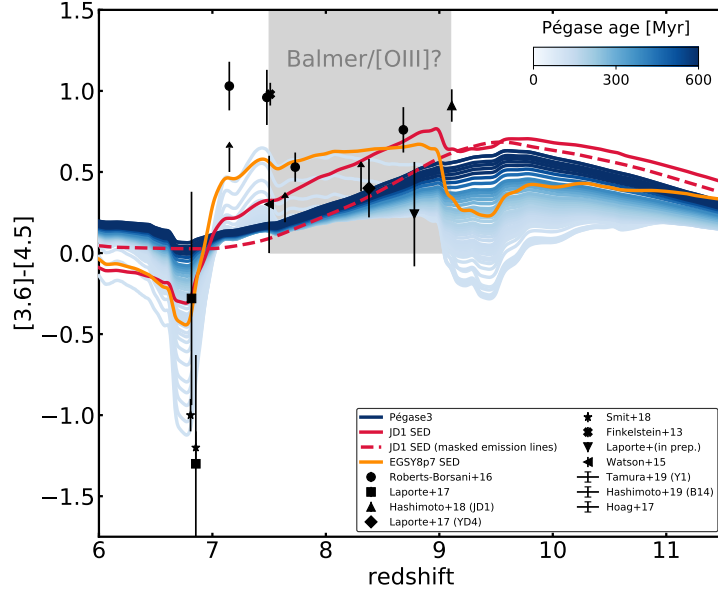


Figure 3. The *Spitzer*/*IRAC* [3.6] - [4.5] colour evolution as a function of redshift. Black points represent spectroscopically confirmed galaxies at $z > 7$ with red *IRAC* colours (see Table 1) with additional data for $z \sim 6.6$ sources with blue *IRAC* colours. The evolution for the synthetic spectra of EGSY8p7 (orange), JD1 (red, solid), JD1 with masked emission lines (red, dashed) can be compared with synthesis models including line emission from Pégase3 (blue shades) for a variety of galaxy ages, assuming a constant SFR from $z = 15$ to $z = 2$. The light gray shaded region highlights an approximate redshift interval over which ambiguity exists as to the primary mechanism for red *Spitzer*/*IRAC* colours.

ID	z_{spec}	H_{160}	$3.6\mu\text{m} - 4.5\mu\text{m}$	Reference
MACS1149_JD1	9.11	25.70 ± 0.01	0.91 ± 0.10	Hashimoto et al. (2018)
GN-z10-3	8.78	26.74 ± 0.12	0.24 ± 0.32	Laporte et al. (in prep.)
EGS8p7	8.68	25.26 ± 0.09	0.76 ± 0.14	Zitrin et al. (2015)
A2744_YD4	8.38	26.42 ± 0.04	0.4 ± 0.18	Laporte et al. (2017a)
MACS0416_Y1	8.31	26.04 ± 0.05	> 0.38	Tamura et al. (2019)
EGS-zs8-1	7.73	25.03 ± 0.05	0.53 ± 0.09	Oesch et al. (2015)
MACS1423-z7p64	7.64	25.03 ± 0.10	> 0.19	Hoag et al. (2017)
z8_GND_5296	7.51	25.55 ± 0.07	0.98 ± 0.07	Finkelstein et al. (2013)
A1689-zD1	7.50	24.70 ± 0.10	0.30 ± 0.30	Watson et al. (2015)
EGS-zs8-2	7.48	25.12 ± 0.05	0.96 ± 0.17	Roberts-Borsani et al. (2016); Stark et al. (2015)
COSY	7.15	25.06 ± 0.06	1.03 ± 0.06	Stark et al. (2015)
B14-65666	7.15	$24.60^{+0.3}_{-0.2}$	> 0.5	Hashimoto et al. (2019)

Table 1. A list of spectroscopically confirmed galaxies at $z > 7$ with red *IRAC* colours.

ID	z_{spec}	μ	$\lambda_{[\text{O III}]}$ [μm]	[O III] integrated flux [Jy km/s]	[O III] FWHM [km/s]	λ_{cont} [μm]	continuum flux Jy
MACS1149_JD1	9.11	10	893.86	0.229 ± 0.050	154 ± 39	917.63	< 3.54
A2744_YD4	8.38	2	829.55	0.030 ± 0.008	49.8 ± 4.2	842.70	9.90 ± 2.30
MACS0416_Y1	8.31	1.43	823.32	0.660 ± 0.160	141 ± 21	850.57	13.70 ± 2.60
B14-65666	7.15	–	720.78	1.500 ± 0.180	429 ± 37	733.68	47.00 ± 12.80

Table 2. A list of $z > 7$ galaxies from Table 1 with [O III] $88\mu\text{m}$ detections and dust continuum constraints (detections and non-detections) from ALMA Band 7 observations. The columns represent, from left to right: the redshift of the galaxy, the assumed magnification factor, the observed wavelength of the [O III] $88\mu\text{m}$ detection, its integrated flux, and the measured FWHM. The last two columns are the central observed wavelength of the dust continuum observations and the associated flux. All error bars and upper limits quoted here are 2σ .

continuum detections, whilst simultaneously reproducing the *HST* photometry, *Spitzer*/*IRAC* excess, and [O III] $88\mu\text{m}$ flux, within the error bars. For Y1 and B14, on the other hand, the *HST* photometry and *Spitzer*/*IRAC* excess are well reproduced, but the models are unable to simultaneously match both the [O III] $88\mu\text{m}$ flux

and dust continuum (in the case of B14, the [O III] $88\mu\text{m}$ flux is matched but the dust continuum is underpredicted, and in the case of Y1 the [O III] $88\mu\text{m}$ flux is underpredicted and dust continuum overpredicted). In comparing these fits to those assuming a single-component only, although the *HST* photometry can be reasonably

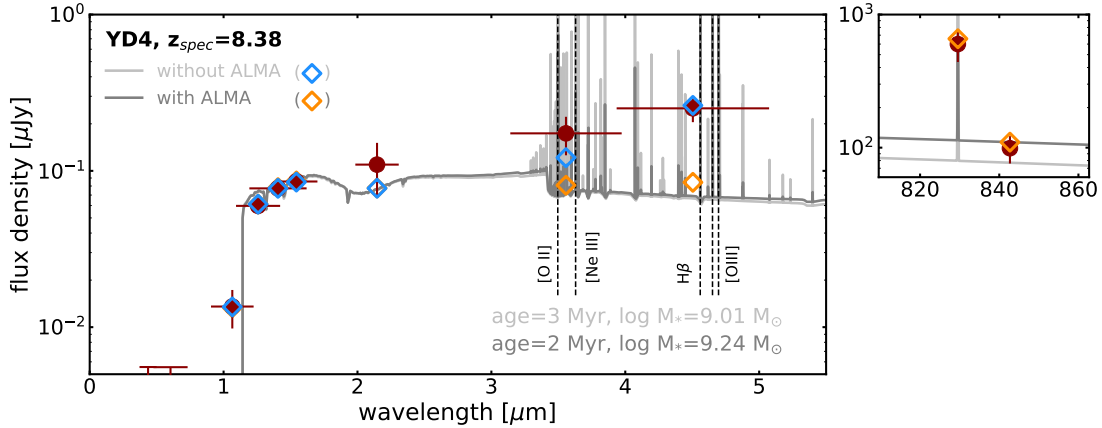


Figure 4. SED fits to the spectroscopically confirmed galaxy, YD4, with *HST*, VLT/HAWK-I K_s and *Spitzer*/IRAC photometry (red points and error bars) and single models of dusty 1-10 Myr Pégase3 spectra. The suite of young Pégase3 spectra are fit once without the ALMA Band 7 spectroscopic observations (light gray line and blue points) and once with them (dark gray line and orange points), both with the strength of nebular emission lines as a free parameter in addition to their stellar masses. The IRAC excess is well fit by contributions from nebular emission lines without inclusion of the ALMA data. However when such constraints are included, the nebular emission is suppressed and cannot account for the excess flux in the *Spitzer*/IRAC 4.5 μm band. Thus, a secondary component arising from starlight is necessary to match the data.

well-reproduced for JD1 and YD4, the single-component fits fail to simultaneously reproduce both the ALMA constraints and the *Spitzer*/IRAC excess. In the cases of Y1 and B14, the ALMA constraints are better matched by the one-component fit, however the *Spitzer*/IRAC excess is only partially matched.

In our two-component fits, a sizeable contribution to the IRAC flux arises from a more mature stellar component. For JD1, YD4 and Y1, the contribution to the IRAC fluxes from the recent burst of star formation is only $\sim 10\text{-}30\%$ and the older component (characterised by Balmer ratios of ~ 2) dominates the flux at $\gtrsim 70\%$. This is due primarily to the relative weakness of the $[\text{O III}]+\text{H}\beta$ lines, for which we measure an equivalent width, $\text{EW}([\text{O III}]+\text{H}\beta) \approx 25\text{-}106 \text{ \AA}$ (compared to $\text{EW}([\text{O III}]+\text{H}\beta) \approx 450\text{-}7700 \text{ \AA}$ for a single-component). The exception to this trend is B14, whose IRAC fluxes remain dominated by the younger component by $\sim 60\text{-}75\%$ ($\text{EW}([\text{O III}]+\text{H}\beta) \approx 200 \text{ \AA}$ for the two-component model and $\text{EW}([\text{O III}]+\text{H}\beta) \approx 3460 \text{ \AA}$ for the one-component model). The total stellar mass (corrected for lensing for those lensed sources) for all of these fits range from $\log M_* = 8.88\text{-}10.19 M_\odot$, with virtually all of the total stellar mass also coming from the earlier period of star formation and the most recent burst contributing primarily through the presence of weak-to-moderate nebular emission.

Furthermore, we also note a difference in the ages of the galaxies, as determined by the onset of the earlier burst in the two-component model or the age of the single-component model. We find an increase in age for each of the four galaxies when multiple components are used, with ages of 80, 260, 140 and 20 Myrs characterising the two-component fits of JD1, YD4, Y1, and B14, and such ages decreasing down to 1, 2, 1 and 3 Myrs assuming on a single burst of recent star formation. In the case of Y1, the age estimate from the two-component fit is in fact a lower limit, since we only have an upper limit for the *Spitzer*/IRAC 3.6 μm photometry. We note here that our preferred $\tau_{\text{old}} = 10$ Myrs value and the galaxy age estimate for JD1 are somewhat lower than those estimated by Hashimoto et al. (2018), whose best fit comprises an older stellar population with an episode of star formation lasting $\tau_{\text{old}} = 100$ Myrs and a galaxy age of 290^{+190}_{-120} Myrs. However, as in their analysis, we find considerable statistical similarity with the

best two-component fit assuming $\tau_{\text{old}} = 100$ Myrs, in which case our age estimate increases to 140 Myrs, closer to the lower limit of their assumed value.

Finally, to enable a quantitative comparison of the one- and two-component fits we examine the log-likelihoods and find, with the exception of Y1, that the two-component fits of each of the galaxies is considered a better fit. However, given the obvious danger of concluding better fits with an additional component with further free parameters, we compare the goodness-of-fit via a comparison of their Bayesian Information Criteria (BIC), which uses the log-likelihoods whilst penalising for additional free parameters. With this consideration, the additional free parameters in the fit to the B14 data are sufficiently penalised to justify only the one-component fit. Whilst such comparisons no doubt gloss over the complexities of defining the birth of such galaxies, they serve as an important illustration of the potential consequences from overlooking the consideration of multiple episodes of star formation. We provide a summary of the above comparison and the main properties of our fits in Table 3.

4 DISCUSSION

We have shown that a Balmer break, arising from a mature stellar population, may be a significant contributor to the IRAC excess seen in spectroscopically-confirmed $z > 7$ star-forming galaxies. While our analysis does not rule out the possibility that much of this excess arises, as has been conventionally assumed, from intense $[\text{O III}]$ emission, using ALMA $[\text{O III}]$ 88 μm emission and dust mass measures, we have examined whether we can constrain the relative contributions of starlight and line emission.

The distinction between intense line emission, attributed to recent episodes of star formation from a young (≤ 10 Myr) stellar population, and a prominent Balmer break consistent with more mature stars, is important in considerations of the early assembly history of galaxies. Both the stellar masses and earlier star formation histories will differ depending on the relative contributions and this, in turn, will affect the inferred star formation activity beyond

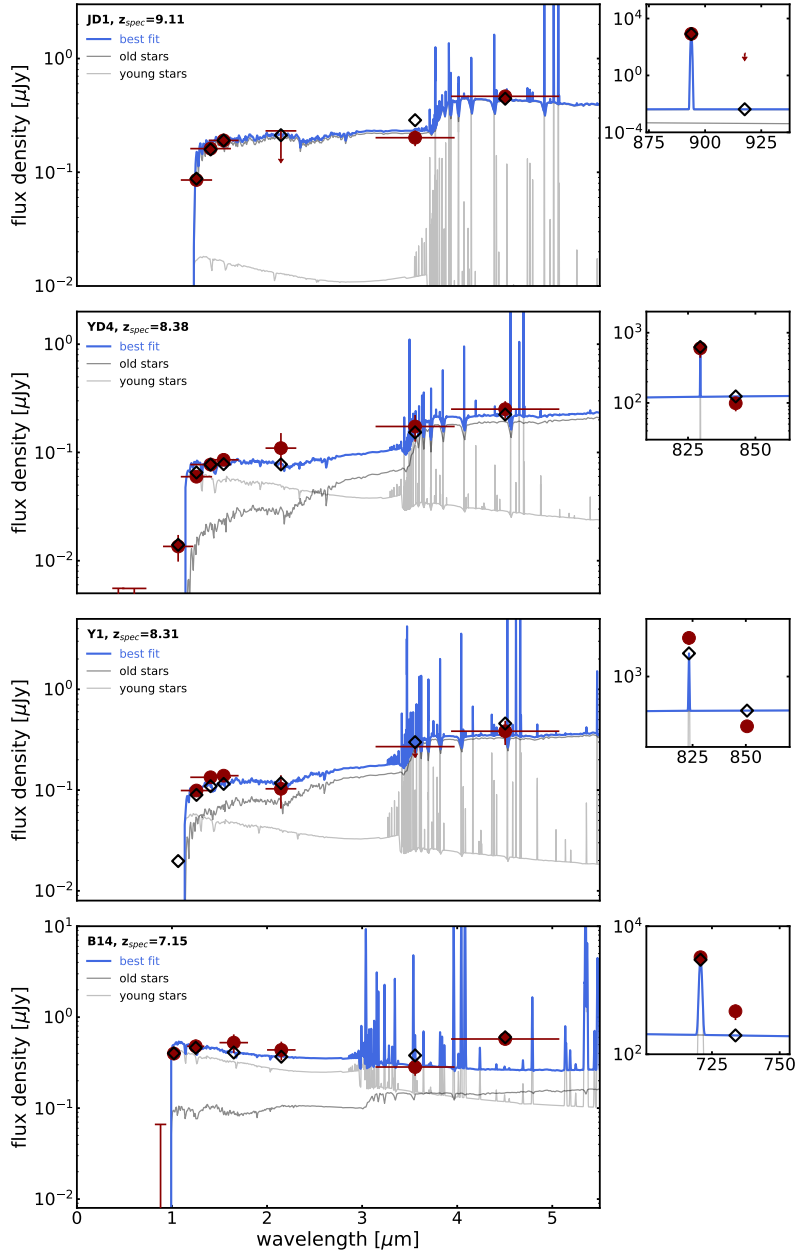


Figure 5. The best fit two-component SED models (blue lines and black points) to observed data (dark red circles and error bars) from *HST*/VISTA + VLT/HAWK-I K_s + *Spitzer*/IRAC photometry (left) and ALMA spectroscopy (upper right inset) for galaxies at $z > 7$ with red *Spitzer*/IRAC colours (JD1, YD4, Y1 and B14). The total fit consists of contributions from both old (darker gray) and young (lighter gray) stars.

the current *HST* redshift horizon of $z \approx 10$. This was first demonstrated for the $z = 9.11$ galaxy JD1 by Hashimoto et al. (2018) where the IRAC excess must arise primarily from starlight, leading to a stellar mass of $4.2 \pm 1.0 \times 10^9 M_\odot$ (lens-corrected for the preferred gravitational magnification) only ≈ 550 Myr after the Big Bang with an implied epoch of first star formation as early as $z \sim 15$.

As an illustration, if we adopt the significant contribution to the IRAC excess from starlight for those $z > 7$ sources in Table 2 for which we fit two-components, their stellar masses increase by an average factor of ≈ 30 compared to contributions from young starlight alone. Although a single-component fit is probably an extreme comparison in this context, nonetheless our two-component fits with an earlier period of star formation must imply an assem-

bly history beyond $z \approx 10$, as discussed by Hashimoto et al. (2018), with interesting consequences for the interpretation of 21cm experiments (Bowman et al. 2018) and the timing of “cosmic dawn”. In Figure 6, we plot the fractional stellar mass assembly history, averaged over our 4 galaxies, up to the epoch of observation in which it can be seen that $\sim 44\%$ of the stellar mass was produced before a redshift $z \approx 10$. Although clearly a modest sample restricted largely to the brightest studied sources at $z > 7$, we can compare this fractional mass assembly history with the prediction of two star formation histories for galaxies with SFRs $> 0.7 M_\odot \text{yr}^{-1}$ discussed by Oesch et al. (2014) similarly normalised at the mean redshift of our galaxies. Whilst the uncertainties are large due to small number statistics, if our galaxies are representative this would indicate

	JD1		YD4		Y1		B14	
	1-comp	2-comp	1-comp	2-comp	1-comp	2-comp	1-comp	2-comp
τ_{old} [Myrs]	–	10	–	200	–	100	–	10
galaxy age [Myrs]	1	80	2	260	1	140	3	20
$M_{*,\text{young}}/M_{*,\text{old}}$	–	2×10^{-3}	–	3.2×10^{-3}	–	1.9×10^{-3}	–	8×10^{-2}
$\log M_{*,\text{total}}$ [M_{\odot}]	8.23 ± 0.01	9.88 ± 0.01	8.71 ± 0.02	10.26 ± 0.06	8.93 ± 0.01	10.35 ± 0.03	9.25 ± 0.04	9.49 ± 0.99
EW([O III]+H β) [\AA]	7668 ± 793	106 ± 43	448 ± 133	25 ± 9	7307 ± 1211	51 ± 11	3462 ± 720	198 ± 260
D_n4000	0.55 ± 0.01	1.94 ± 0.02	0.77 ± 0.00	2.09 ± 0.07	0.81 ± 0.01	1.99 ± 0.02	0.82 ± 0.01	0.97 ± 0.35
3.6 μm flux contribution		(9.8, 90.2) %		(25.4, 74.6) %		(23.9, 76.1) %		(62.4, 37.6) %
4.5 μm flux contribution		(8.2, 91.8) %		(18.4, 81.6) %		(30.8, 69.2) %		(75.5, 24.5) %
log-likelihood	-188.81	-12.22	-9.44	-3.02	-62.47	-66.92	-6.17	-4.86
BIC	403.21	62.84	44.02	43.76	150.33	171.94	38.10	48.37

Table 3. Summary of the main properties and parameters (uncorrected for any lensing of the objects) of the favoured one- and two-component SED fits determined by our SED fitting code with Pégase3 spectra. The tabulated flux percentages for the two-component models in the middle section of the table are the relative contributions from the (young,old) components to the total flux measured in that band.

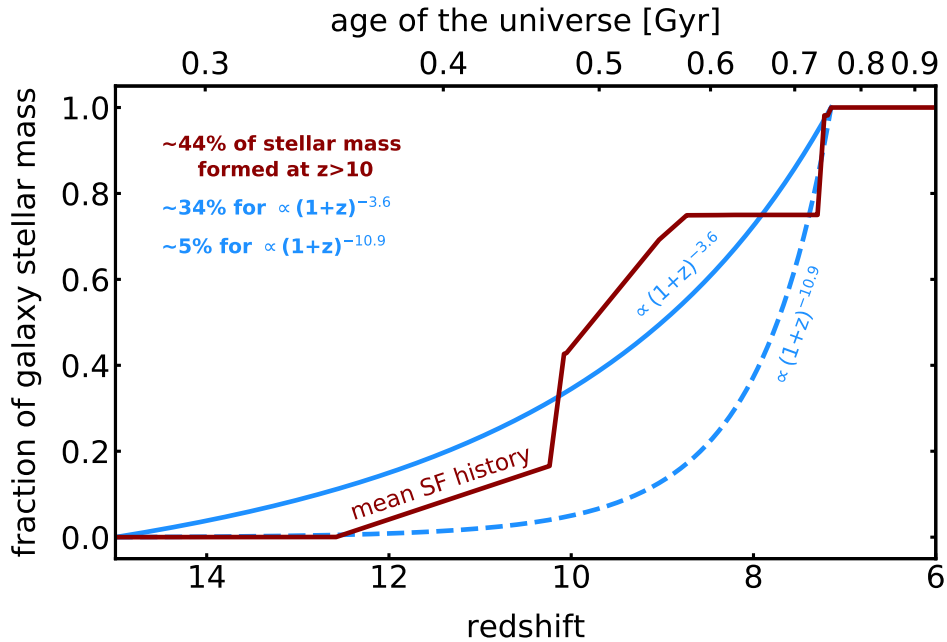


Figure 6. The fractional stellar mass assembly history averaged over the four galaxies in Table 2 (dark red), adopting the best two-component fits in Figure 5. The solid and dashed blue lines represent the equivalent fractional histories for the two cosmic SFR density relations presented in Figure 9 of Oesch et al. (2014).

a more gradual decline in the star formation history beyond $z \approx 8$ than Oesch et al. (2014) prefer (see McLeod et al. 2016). Whilst clearly a simplistic comparison, it serves to emphasise the importance of determining the true origin of the IRAC excess in $z > 7$ galaxies. Ultimately NIRSPEC on JWST will be well-placed to resolve the ambiguities explored in this paper via direct spectroscopy of a large sample of $7 < z < 9$ galaxies securing not only the strength of rest-frame optical lines such as [O III] 5007 \AA but also absorption line measures such as H δ which is a further indicator of stellar ages.

ACKNOWLEDGEMENTS

We thank Rychard Bouwens, Ivo Labbé and Dan Stark for useful discussions regarding the interpretation of *Spitzer*/IRAC colours. We would also like to thank Michel Fioc and Brigitte Rocca-Volmerange for their help in generating Pégase3 models, as well as Isabella Lamperti for illuminating discussions on developing the SED-fitting code and Roger Wesson for valuable conversations regarding the [O III] line ratio. The authors acknowledge funding from the European Research Council (ERC) under the European Union Horizon 2020 research and innovation programme (grant agreement No 669253). NL acknowledges support from the Kavli foundation.

REFERENCES

- Atek, H., Richard, J., Kneib, J.-P., et al. 2015, *ApJ*, 800, 18
- Bingelli, C., Zackrisson, E., Xiangcheng, M. et al. 2019, *MNRAS*, 489, 3
- Bouwens, R. J., Illingworth, G. D., Oesch, P. A., et al. 2015, *ApJ*, 803, 34
- Bowman, J. D., Rogers, A. E. E., Monsalve, R. A., et al. 2018, *Nature*, 555, 67
- Bradley, L. D., Zitrin, A., Coe, D., et al. 2014, *ApJ*, 792, 76
- Chabrier, G. 2003, *PASP*, 115, 763
- Coe, D., Salmon, B., Bradač, M., et al. 2019, *ApJ*, 884, 85
- Ellis, R. S., McLure, R. J., Dunlop, J. S., et al. 2013, *ApJ*, 763, L7
- Finkelstein, S., Papovich, C., Dickinson, M. et al. 2013, *Nature*, 502, 524
- Fioc, M., & Rocca-Volmerange, B. 2019, *A&A*, 623, A143
- Grogin, N. A., Kocevski, D. D., Faber, S. M., et al. 2011, *ApJS*, 197, 35
- Hashimoto, T., Laporte, N., Mawatari, K., et al. 2018, *Nature*, 557, 392
- Hashimoto, T., Inoue, A., Mawatari, K. et al. 2019, *PASJ*, in press
- Hoag, A., Bradač, M., Trenti, M., et al. 2017, *Nature Astronomy*, 1, 0091
- Katz, H., Laporte, N., Ellis, R. et al. 2019, *MNRAS*, 484, 4054
- Koekemoer, A. M., Faber, S. M., Ferguson, H. C., et al. 2011, *ApJS*, 197, 36
- Labbé, I., Oesch, P. A., Bouwens, R. J., et al. 2013, *ApJ*, 777, L19
- Laporte, N., Ellis, R. S., Boone, F., et al. 2017, *ApJ*, 837, L21
- Laporte, N., Nakajima, K., Ellis, R. S., et al. 2017, *ApJ*, 851, 40
- Lotz, J. M., Koekemoer, A., Coe, D., et al. 2017, *ApJ*, 837, 97
- Maseda, M. V., van der Wel, A., Rix, H.-W., et al. 2014, *ApJ*, 791, 17
- Matthee, J., Sobral, D., Boone, F., et al. 2017, *ApJ*, 851, 145
- McLeod, D. J., McLure, R. J., & Dunlop, J. S. 2016, *MNRAS*, 459, 3812
- Oesch, P. A., Bouwens, R. J., Illingworth, G. D., et al. 2014, *ApJ*, 786, 108
- Oesch, P. A., van Dokkum, P. G., Illingworth, G. D., et al. 2015, *ApJ*, 804, L30
- Oesch, P. A., Bouwens, R. J., Illingworth, G. D., et al. 2018, *ApJ*, 855, 105
- Oke, J. B., & Gunn, J. E. 1983, *ApJ*, 266, 713
- Pentericci, L., Carniani, S., Castellano, M., et al. 2016, *ApJ*, 829, L11
- Roberts-Borsani, G. W., Bouwens, R. J., Oesch, P. A., et al. 2016, *ApJ*, 823, 143
- Salmon, B., Coe, D., Bradley, L., et al. 2018, *ApJ*, 864, L22
- Sawicki, M. 2012, *PASP*, 124, 1208
- Smit, R., Bouwens, R. J., Franx, M., et al. 2015, *ApJ*, 801, 122
- Smit, R., Bouwens, R. J., Carniani, S., et al. 2018, *Nature*, 553, 178
- Sobral, D., Matthee, J., Darvish, B., et al. 2015, *ApJ*, 808, 139
- Stark, D. P. 2016, *ARA&A*, 54, 761
- Stark, D. P., Richard, J., Charlot, S. et al. 2015, *MNRAS*, 450, 1846
- Stark, D. P., Ellis, R. S., Charlot, S., et al. 2017, *MNRAS*, 464, 469
- Tamura, Y., Mawatari, K., Hashimoto, T. et al. 2019, *ApJ*, 874, 27
- Watson, D., Christensen, L., Knudsen, K. K. et al. 2015, *Nature*, 519, 327
- Zheng, W., Zitrin, A., Infante, L., et al. 2017, *ApJ*, 836, 210
- Zitrin, A., Labbé, I., Belli, S., et al. 2015, *ApJ*, 810, L12

This paper has been typeset from a $\text{\TeX}/\text{\LaTeX}$ file prepared by the author.